This is a previous version of the article published in Lab on a Chip. 2019, 19: 3943-3953. doi:10.1039/C9LC00728H

ARTICLE

Activate Capture and Digital Counting (AC+DC) assay for protein biomarker detection integrated with a self-powered microfluidic cartridge

Received 00th January 20xx,
Accepted 00th January 20xx

DOI: 10.1039/x0xx00000x

Congnyu Che[a], Nantao Li[b], Kenneth D. Long[a], Miguel Ángel Aguirre[c], Taylor D. Canady[d], Qinglan Huang[b], and Brian T. Cunningham[a,b,d,*]

We demonstrate a rapid, single-step, and ultrasensitive assay approach for quantification of target protein molecules from a single droplet test sample. The assay is comprised of antibody-conjugated gold nanoparticles (AuNPs) that are "activated" when they are mixed with the test sample and bind their targets. The resulting liquid is passed through a microfluidic channel with a photonic crystal (PC) biosensor that is functionalized with secondary antibodies to the target biomarker, so that only activated AuNPs are captured. Utilizing recently demonstrated hybrid optical coupling between the plasmon resonance of the AuNP and the resonance of the PC, each captured AuNP efficiently quenches the resonant reflection of the PC, thus enabling the captured AuNPs to be digitally counted with high signal-to-noise. To achieve a single-step assay process that is performed on a single droplet test sample without washing steps or active pump elements, controlled single-pass flow rate is obtained with an absorbing paper pad waste reservoir embedded in a microfluidic cartridge. We use the Activate Capture and Digital Counting (AC+DC) approach to demonstrate HIV-1 capsid antigen p24 detection from a 40 µL test sample at a one million-fold dynamic range (10-10^7 pg mL^{-1}) with only a 30-minute process that is compatible with point-of-care (POC) analysis. The AC+DC approach allows for ultrasensitive and ultrafast biomolecule detection, with potential applications in infectious disease diagnostics and early stage disease monitoring.

Introduction

The requirements of portability, low cost, simple workflow, rapid test results, quantitative output, and low limits of detection (LOD) must be achieved simultaneously for laboratory-based diagnostic assays to transition to point-of-care (POC) environments.[1-3] Among the most challenging POC diagnostic scenarios is the case of a low-concentration target molecule within a low-volume test sample, due to the strictly limited number of analytes available for detection. For example, when serum is derived from a 20-50 µL finger prick of whole blood, > 20 000 different biomarkers of clinical interest will be present at concentrations as low as 10 pg mL^{-1}, which represents only 10^6-10^7 available biomolecules in the test sample for one target.[4] It is well-recognized that the response time required to bind sufficient molecules upon the sensing surface of a biosensing transducer is determined typically by diffusion, which can extend to hours and even to days to generate a signal above the background noise level.[5,6] These principles apply fundamentally to all sensors that accumulate and concentrate target molecules onto a transducer, including fluorophore-tagged molecules in microarray spots,[7-9] label-free optical biosensors,[10-13] and impedance-based sensors.[14-16] Integration of sensors with microfluidic channels serves to reduce assay time by constraining the diffusion distance between the molecules in the sample and the sensor, and to create laminar flow over the sensor to distribute target molecules broadly.[17]

Due to the inability of conventional transducers to efficiently capture and to directly quantify low numbers of captured molecules, amplification of the number of detectable molecules (for example, with Polymerase Chain Reaction (PCR)) or the signal from each captured molecule (for example, with Enzyme Linked Immunosorbent Assays (ELISA)) has been used effectively to achieve reduced detection limits.[18] However, these amplification approaches require additional reagents (such as enzymes), thermal cycling (for PCR) and multiple washing steps (for ELISA) which results in complex workflows that are not fully compatible with low-resource POC settings.

In this work, we report an assay approach that simultaneously meets the requirements of a POC assay through the combined use of plasmonic nanoparticle tags and an imaging-based optical biosensor embedded in a microfluidic cartridge. We utilize a novel form of biosensor microscopy in which the entire surface of a photonic crystal (PC) serves as an

[a] Department of Bioengineering, University of Illinois at Urbana-Champaign, 208 North Wright Street, Urbana, IL 61801, USA.
[b] Department of Electrical and Computer Engineering, University of Illinois at Urbana-Champaign, 208 North Wright Street, Urbana, IL 61801, USA.
[c] Department of Analytical Chemistry and Food Science and University Institute of Materials, Faculty of Science, University of Alicante, P.O. Box, 03080 Alicante, Spain.
[d] Carl R. Woese Institute for Genomic Biology, University of Illinois at Urbana-Champaign, 1206 West Gregory Drive, Urbana, IL 61801, USA.
Electronic Supplementary Information (ESI) available: [details of any supplementary information available should be included here]. See DOI: 10.1039/x0xx00000x

active transducer that can be quickly imaged over a substantial area. High contrast digital resolution sensing of analytes is obtained through the use of plasmonic gold nanoparticle (AuNP) tags that support localized surface plasmon resonance (LSPR) which spectrally overlaps with the resonance reflection of the PC. Through a plasmonic–photonic hybrid coupling between the PC and AuNPs, localized quenching of resonantly reflected light is used to detect individual bound AuNP tags onto the PC surface.[19] We refer to this detection method as Photonic Resonant Absorption Microscopy (PRAM), as we gather magnified images of changes in the reflected Peak Intensity Value (PIV) from the PC while we record the spatial distribution of AuNP-tagged analyte on the PC with single-analyte precision.[20]

The assay approach described in this work incorporates a second important feature that enables a single-step workflow and a high degree of selectivity. At the first stage of the assay, the test sample is mixed with an excess of antibody-functionalized AuNPs which specifically bind to the target antigens (Figure 1a). Therefore, for a low concentration of the target, only a small fraction of the AuNP population will be "activated". Next, the mixture is introduced into the inlet port of the microfluidic cartridge, and driven toward the sensing region by capillary force created by an absorbing pad, to yield a controlled flow rate (Figure 1b). The PC biosensor is prepared with spatially separate regions designated as "reference" or "active" (Figure 1c). The PC active region is functionalized with surface-immobilized detection antibodies that bind activated AuNPs, while inactive AuNPs flow past without being captured. In order to account for the possibility of nonspecific capture of inactivated AuNPs, the reference region is prepared with a "blocked" surface without the detection antibody. After running the test sample through, the capture process can be monitored over time with a sequence of scans of the same active and reference regions of the PC using PRAM (Figure 1d). Surface-captured AuNPs in the PRAM image can be enumerated with single AuNP precision, with the expectation that each bound AuNP in the active region represents at least one target biomolecule. We call the entire assay method "Activate Capture and Digital Counting" (AC+DC).

This work represents the first utilization of the AC+DC assay approach for detection of a protein target molecule. Our initial demonstration of AC+DC was performed in the context of ultrasensitive detection of specific miRNA sequences in buffer and serum, in which the activated AuNP solution was applied to a PC within a stagnant ~10 µL microwell volume.[21] While we achieved 100 aM LOD, the capture process was limited by diffusion, and thus up to two hours were required to detect the lowest concentration. In this work, we seek to demonstrate AC+DC in a workflow that is compatible with POC applications, especially reducing the time requirements for a diffusion-limited assay. We integrated the PC sensor within a microfluidic channel that enables the activated AuNP solution to be flowed over the sensor from the top, while PRAM imaging is conducted from below, through a transparent substrate. The restricted ~25 µm height of the microfluidic channel is designed in concert with a flow rate of ~1.33 µL/min to yield a ~18% AuNP capture efficiency, predicted by analytical and computational models. Thus, a low-volume test sample of 40 µL moves past the sensor in a single pass, for a ~30-minute assay time. Importantly, we modulate the flow rate using an absorbing paper pad that is placed at the waste reservoir downstream of the PC sensor, so that no complex pump/valve components or pneumatic pressure sources are required to drive the test sample. The composition and dimensions of the absorbing pad were engineered to deliver a desired flow rate, and to accommodate the test sample volume easily.[22-24]

By combining the AC+DC assay approach with a self-powered microfluidic cartridge, our goal is to provide a pathway toward a simple, yet highly sensitive, selective, and quantitative assay for biomarker proteins that is compatible with all the requirements for POC environments. In this paper, we summarize the PRAM imaging approach, the design/fabrication of the PC biosensor, and the design of the microfluidic cartridge. As a proof-of-concept, we begin characterization of the AC+DC approach through the use of pre-activated AuNPs prepared with anti-mouse IgG that are captured by a PC prepared with IgG. Subsequently, as a representative example of using AC+DC in the context of a sandwich assay, we demonstrate detection of HIV-1 capsid (p24) antigen in buffer, using anti-p24 monoclonal antibody conjugated AuNPs and a PC active region functionalized with secondary anti-p24 monoclonal antibody. We achieve detection of p24 antigen from a 40 µL test sample through a one million-fold dynamic range (10-10^7 pg mL^{-1}) and a detection limit of 10 pg mL^{-1} in only 30 minutes.

PC biosensor design and PRAM imaging

Sensitive detection and specific biomolecule labelling enables spatially distributed individual analytes in the test sample to be sensed with a high signal-to-noise ratio. Our approach utilizes a PC biosensor that provides sensitivity over an extended surface area in conjunction with an imaging detection instrument.

A PC biosensor is a sub-wavelength periodic surface structure that is designed to function as a highly efficient narrow bandwidth resonant reflector. The PC structure used in our work is comprised of low refractive index material (UV-cured polymer, UVCP) that is coated with a higher refractive index material (TiO2) as shown in Figure 2a. When the PC is illuminated at normal incidence with a broadband light source, the resonant wavelength is reflected with nearly 100% efficiency while all other wavelengths are transmitted.[25] PCs were fabricated on glass cover slips (Thermo Scientific, 24×60 mm^2) by room temperature nanoreplica molding as described in prior publications.[26] Briefly, a quartz reticle with a negative image of the desired PC linear surface structure (period = 400 nm, depth = 120nm) was applied to mold the liquid UVCP on the glass cover slip. After exposure to a high intensity UV lamp for 80 seconds (Xenon), the UVCP was cured, and the quartz template was removed, resulting in transfer of the periodic surface pattern to the cover slip. Finally, a thin layer of TiO2 (refractive index = 2.35, thickness ~70 nm) was deposited by reactive RF sputtering (PVD 75, Kurt Lesker). The resulting PC covers a surface area of 9×9 mm^2. The PC is designed to

function as a narrowband optical resonator that optimally reflect λ=625 nm under aqueous immersion.[10]

Recent publications from our group have demonstrated the implementation of detection instruments that spatially analyze the resonantly reflected Peak Wavelength Value (PWV) and PIV to generate biosensor images for the detection of proteins, nucleic acids, cells, and nanoparticles attached to the PC surface.[9,10,27,28] Interestingly, the reflected resonant intensity has been shown to be locally reduced by the presence of surface-attached objects through distinct mechanisms of outcoupled scattering[20] or by optical absorption[10]. We have also experimentally demonstrated a mechanism through which optical absorption of a PC-attached nanoparticle can be substantially enhanced through a mechanism of "hybrid coupling",[19,29] which occurs when the plasmon resonant wavelength of a metallic nanoparticle is selected to match the resonant reflection wavelength of the PC.

In the PRAM imaging method, the hybrid resonator optical absorption is used as the contrast mechanism for image-based detection of objects attached to a PC biosensor surface. Here, we choose commercially available gold nano-urchin nanoparticles (0.04 μg/μL, Cytodiagnostics) of 90 nm diameter, which display a LSPR wavelength of 630 nm, to coincide closely with the 625 nm resonant wavelength of our PC. The AuNP has a rugged exterior surface (high surface area to volume ratio) to facilitate attachment of a high density of capture molecules.

A schematic diagram of the PRAM instrument is shown in Figure 2a. The system is built upon the body of a bright field microscope (Carl Zeiss Axio Observer Z1) with 10× or 40× objective lens as described previously.[10] The optical components consist of an optical fibre-coupled broadband light-emitting diode (LED) (Thorlabs M617F1, 600 < λ< 650 nm) source, a polarizing beam splitter (PBS) to collimate and filter the fiber output and a cylindrical lens (f = 200 mm) to focus the polarized light onto the objective back focal plane. A line-profiled light beam which is perpendicular to the PC grating lines illuminates the PC from below at normal incidence through the microscope objective. The reflected spectrum passes through the inverted objective lens and through a narrow slit aperture (width = 30 μm) of an imaging spectrometer (Acton Research). Finally, reflected light from the illumination line on the PC surface is collected by a charge-coupled device camera (Photometrics Cascade, 512×512 pixels).

The resonant reflection spectra from one pixel of a PRAM image is shown in Supplementary Figure 1 with and without an attached AuNP. We observe a ~22% reduction in reflection efficiency by the absorption of one AuNP in the pixel area. Each pixel represents a ~0.1×0.1 μm^2 area of the PC, when an instrument is utilizing a 40× objective.

Design and fabrication of the microfluidic cartridge

The self-powered microfluidic cartridge was inspired by previously described approaches in which vacuum compartments,[30-32] capillary microstructures[33-36] or absorbing materials[22-24] were used to drive liquid flow through the channels, thus avoiding the requirement for external pressure sources (such as syringes, compressed air, and electro-pneumatic systems[37,38]) or integrated microfluidic pumps/valves. We constructed the microfluidic cartridge with Polymethyl-methacrylate (PMMA, also commonly called "acrylic" or "plexiglass", thickness = 0.76 mm and 4.75 mm, Ridout Plastics) because it is optically transparent, non-porous, inert in aqueous solution, and not hydrolyzed during use with aqueous solvents.[39] Optically clear adhesive films (OCA, 3M 8211, thickness = 25 μm) were selected to provide adhesion between adjacent PMMA layers. A computer-controlled laser cutter (Epilog Fusion 40) was used to cut through PMMA sheets or adhesive sheets to produce openings in specific locations.

The fully assembled microfluidic cartridge is 75 mm long, 25 mm wide, and 7 mm thick (Figure 2b). An expanded schematic of the cartridge components is shown in Figure 2c. The thin PMMA sheet on top contains an inlet hole (diameter = 3 mm) and an outlet hole (diameter = 1 mm), followed by an adhesive layer to provide a connecting channel between the gas-escaping hole and the gas outlet. Addition of this OCA layer ensures sealing of the test sample, which is critical for handling various samples containing biohazard materials, such as a serum specimen. The thicker PMMA sheet provides a reservoir for the test sample while also providing a mechanically stable platform that prevents the assembly from twisting or bowing. A stack of two thin PMMA sheets with laser cutouts provides a cavity for holding the absorbing pad in place. The bottom-most adhesive layer is used to create a tunnel that connects the inlet to a 25 μm height sample channel that passes over the PC biosensor, followed by a serpentine channel leading to the absorbing pad. The length and width of the serpentine channel is designed to provide resistance to the absorbance-driven flow. A custom-designed pressing fixture was constructed to enable all the layers to be stacked precisely, and to apply a uniform and reproducible adhesion force controlled with a torque wrench. The absorbing paper material (Ahlstrom, grade 610, thickness = 0.18 mm, retention = 1.5 μm) was cut to size (width = 0.7 cm, length = 3.5 cm) by hand with a razor knife. Through experimentation, we determined that nine layers of vertically stacked filter paper formed an absorbing pad (thickness = 1.62 mm, capacity = 150 μL) provided sufficient volume capacity and flow rate for our application. Assembled cartridges were stored for at least 48 hours before use, to ensure that delamination would not occur during biological experiments. As a final assembly step before performing sensing experiments, the functionalized PC biosensor (9×9 mm^2), fabricated on a glass cover slip (Thermo Scientific, 24×60 mm^2) is attached to the bottom-most adhesive layer. However, the sample only flows over a 0.5×9 mm^2 region of the PC biosensor, where the reference and active regions will be imaged by PRAM.

The microfluidic cartridge is organized into four functional units: the sample reservoir, the sample channel, the serpentine resistance channel and the absorbing pad. The sample liquid inside the cartridge is manipulated by a combination of several forces. After loading liquid into the sample reservoir, capillary force created by the confined sample channel (0.5 mm wide)

together with pressure difference between the inlet (with sample loaded) and the outlet hole at atmospheric pressure attracts the fluid to the leading edge of the PC. As the sample flows over the PC, activated AuNPs will be captured by immobilized antibodies in the active sensing region. The linear periodic surface structure of the PC is oriented parallel to the flow direction, and further draws the sample into the biosensor channel via capillary force.[34] The serpentine channel creates flow resistance that is proportional to its length, and inversely proportional to the channel cross section area.[40-42] Finally, when the fluid reaches to the absorbing pad, the wicking force provides the dominant force to pull the remaining test sample volume through the cartridge.

Surface functionalization of PCs and Antibody-conjugation to AuNPs

The PC surface was cleaned by sonication in a series of separate glass containers of acetone, isopropyl alcohol (IPA), and Milli-Q water for two minutes each, followed drying in a stream of N_2 gas, and O_2 plasma treatment (Pico plasma system, diener electronic, power = 100%, time = 10 minutes) to remove any residual organic materials and to facilitate the attachment of temporary poly(dimethylsiloxane) (PDMS). To facilitate surface functionalization of the reference and active regions, the PC surface was coated with a layer of (3-Glycidyloxypropyl) trimethoxysilane (GPTMS, Sigma Aldrich) in a 80 °C vacuum oven overnight.[43] After rinsing the silane solution from the PC surface using toluene, methanol and Milli-Q water, two PDMS wells (diameter = 3 mm) were applied onto the PC surface to separate the reference and active areas. For the proof-of-concept IgG capture assay, we incubated 13 µL of blocking agent (StartingBlock in PBS, Thermo Scientific) in the reference area, and 13 µL of Mouse IgG (0.4 µg/µL, ab37355, Abcam) in the active area for 12 hours. After washing the wells with PBS twice, 13 µL of blocking agent was added into both wells to block unattached sites for 24 hours. For the HIV-1 capsid p24 antigen detection assay, we incubated 26 µL of blocking agent in the reference area, and 26 µL of anti-p24 monoclonal antibody (0.25 µg/µL, PM-6335, ProSci) in the active area for 12 hours. After washing the wells with PBS twice, 13 µL of blocking agent was added into both wells to block unoccupied sites for 6 hours. Finally, the prepared PC surface was cleaned again with PBS twice and Milli-Q water followed by drying with N_2 gas. At this stage, the PDMS wells are removed, and the PC is attached to the microfluidic cartridge, so the test sample encounters the reference and active regions in series.

Goat anti-mouse IgG (2 µg/µL, ab6708, Abcam) for the proof-of-concept assay or anti-p24 monoclonal antibody (1 µg/µL, PM-6585, ProSci) for the p24 detection assay was modified with heterobifunctional polyethylene glycol (SH-PEG-COOH, JenKem Technology) and conjugated on 90nm gold nano-urchin AuNPs following a previously published protocol.[10] Aqueous solutions of SH-PEG-COOH, 1-ethyl-3-(3-dimethylaminopropyl) carbodiimide (EDC, Thermo Scientific), and N-hydroxy succinimide (NHS, Thermo Scientific) at an equal molar ratio were mixed with Milli-Q water. The pH of the reaction mixture was adjusted to 7.4 by adding 10 × concentrated phosphate buffer saline (PBS) and NaOH. Afterward, the solution was gently agitated for 1 hour. The mixture was then mixed with 10 µL of the antibody solution (5 µL for the p24 assay), and incubated at room temperature for 2 hours. Subsequently, the mixture was filtered using a centrifuge filter tube (Merck Millipore Ltd) with a 50-kDa filter to remove any unreacted material. The final SH-PEG-Antibody conjugate solution was obtained by rinsing the mixture with PBS buffer (pH 7.4) twice. The maximum coverage of antibodies on AuNPs was prepared by adding 12 µL of SH-PEG-Antibody solution to 200 µL of AuNP solution with incubation for 1 hour, as determined by dynamic light scattering (Supplementary Figure 3).

Results and discussion

Optimization and modulation of the microfluidic cartridge

The pump power of the absorbing pad can be engineered to provide a desired flow rate through the selection of the porous material and its dimensions. Generally, greater pore size of absorbing paper material enables a faster flow rate based on the Hagen-Poiseuille law, which describes laminar flow through a long capillary of uniform circular cross section.[44] We selected a low ash grade filter paper (grade 610, Ahlstrom) that contains more than 95% super-refined alpha-cellulose and linter fibres with a pore size of 1.5 µm to provide a relatively slow flow rate. After the paper material was selected, dimensions of the absorbing pad can be estimated by Darcy's law, which describes flow in a straight paper channel of constant width:[45,46]

$$Q = -\frac{\kappa W H}{\mu L}\Delta P \quad (1)$$

Where Q [m^3/s] is the volumetric flow rate, κ [m^2] is the permeability of the paper to the fluid, µ [Pa·s] is the viscosity of the fluid, W is the width of the paper channel perpendicular to the flow direction, H is the thickness of the paper channel, and ΔP is the pressure difference along the direction of flow over the paper channel length L.

In the microfluidic cartridge, the capillary force of the linear PC grating lines and resistance of channel walls are several orders of magnitude smaller than the wicking force. Therefore, the volume flow rate of the test sample inside the channel will be the same as the rate of sample absorption by the porous media, which is in turn determined by the ratio of the width to the length of paper channel ∂=W/L. We sought to experimentally test the effects of the filter paper pad dimensions on the flow rate as a function of time, using Darcy's law for initial guidance. Because the permeability and the thickness of the paper material is constant, selection of ∂ is the simplest means to adjust the flow rate. We tested three ∂ values of 0.14, 0.23, and 0.39. The flow rates are estimated by measuring the remaining volume of the test sample (colored water) in the inlet port with an adjustable volume micropipette

from 0 to 60 minutes with an increment of 5 minutes. The results are plotted in Figure 3a, where we observe that increasing ∂ provides greater flow rate. Over the course of 60 minutes, the rate of absorption into the pad is fairly constant if we ignore the error bar caused by the uncertainty of handcrafting, and that the ∂ = 0.14, 0.23, and 0.39 pads are capable of completely absorbing volumes of 60, 80, and 120 µL, respectively. We note that, as shown in Figure 3a, the flow rate begins to decelerate as the pad approaches its capacity. Using a linear fit to estimate the average flow rates of the pads, we derive rates of 1.16 µL/min, 1.33 µL/min and 2.17 µL/min, respectively. We further observe that a narrower pad tends to have a more constant flow rate as determined by the standard deviation of the measured flow rate for our 3 independent trials for each ∂ value. For our specific application, we consider a sample volume of 40 µL, which we seek to draw past the PC sensor within a 30-minute time period. Therefore, a 0.7 cm×3 cm absorbing pad was chosen as the most appropriate pad size to meet our requirements, as it provides sufficient excess volume capacity and a constant flow rate of ~1.33 µL/min for 30 minutes that will flow the entire test sample over the sensor.

The microfluidic cartridge provides rapid and efficient capture of antigen-activated AuNPs on the active region of the PC. To provide an estimate of the AuNP capture efficiency, the channel dimensions, flow rate, and sensor dimensions were simulated using a COMSOL model that incorporates the effects of convection, diffusion, and surface capture. In this model, the sample liquid flows through a channel of height H and width W_c, the bottom of the channel contains the PC biosensor of width W_s, and length L_s. The long axis of the sensor is oriented parallel to the flow direction, and the sensor region displays the immobilized capture antibodies. The initial concentration of the analyte at the inlet of the channel is C_o, and diffusivity is D. Details about the governing equations and parameters of the COMSOL simulation we performed can be found in the Supplementary Notes. For simplicity, we assume that the variances in concentration are extremely small along the width of the channel, thus we simplify the 3-D sample channel model to a 2-D cross-section model as Figure 3b shows. The channel height then becomes the essential parameter that influences the flow resistance and the surface capture rate. The 2-D COMSOL model can be used to predict the effects of changes in the channel height as to allow a sufficient number of target molecules to be captured and imaged in a limited time period (e.g. 30 minutes).

Initially, the approximation eqn (2) and eqn (3) derived by Manalis *et al*. can provide an estimate of the total flow time and average capture efficiency, which confirms our intuition that an increased channel height will enable a greater flow rate, but reduces the total AuNPs bound.[17] For simplicity, we assume that AuNPs are instantly and irreversibly captured when they touch the PC surface.

$$T \cong \frac{12\eta LV}{H^3 W_c P} \quad (2)$$

$$R \cong \left(\frac{6\eta^2 L^4 D^2}{H^8 P^2}\right)^{\frac{1}{3}} \quad (3)$$

Where T is the time required to pump the entire sample volume through the channel, R is the fraction of activated AuNPs collected, η is the fluid viscosity, V is the sample volume and P is the pressure applied.

Using eqn (2) and eqn (3) with a 25 µm channel height and a 0.5 mm channel width, an average flow rate of 1.33 µL/min, and a sensor length of 9 mm, we estimate that 18% of the activated AuNPs from a 40 µL volume test sample can be collected during the 30 minutes that the volume flows over the sensor.

In the 2-D COMSOL model, the concentration of captured target biomolecules on the PC biosensor from 0 to 60 minutes with an increment of 10 minutes was calculated. Figure 3c shows the concentration of surface-attached AuNPs along PC sensor accumulate with increasing time. Activated AuNPs are being depleted from solution by their capture on the sensing part of the PC surface, and due to depletion, the highest density of surface-captured AuNPs occurs at the leading edge of the PC active region, with the concentration of captured AuNPs decreasing exponentially downstream from the leading edge. Therefore, we may accordingly choose the location of PRAM imaging at the location of highest predicted AuNP during each experiment to ensure accurate and consistent results. Figure 3d shows the concentration of the target AuNPs in the volume above the PC biosensor in the 2D domain after 60 minutes. From the zoomed-in figure of the center of the total PC active area, we observe a depletion zone almost occupies one fifth of the whole channel, which is coincident with the results calculated by the analytical model. In conclusion, with a 25 µm channel height and a 0.7 mm × 3 mm absorbing pad, the microfluidic cartridge can pump 40 µL of sample volume in 30 minutes and capture nearly 20% of the activated AuNPs in the test sample. The capture efficiency can be greater than 20%, but through the trade-off of lower flow rate, which in turn will require substantially longer assay times.

Detection of biomolecules using AC+DC

As a proof-of-concept of microfluidic digital biomolecule detection, we investigated AuNP-anti-mouse IgG detection with a PC biosensor prepared with immobilized mouse IgG. Using this combination of molecules on the AuNP and the PC, each AuNP is considered to be "active" with respect to the complementary binding protein on the PC. We added 40 µL of serially diluted concentrations of AuNP-anti-mouse IgG solution into a set of microfluidic devices and scanned the respective PC biosensor at 15 minute intervals up to 60 minutes. The starting concentration of the AuNP purchased from Cytodiagnostics is 8.92 pM, representing 5.37×10^6 AuNPs/µL. After the anti-mouse IgG conjugation, the AuNP conjugate solution was diluted into 0.5×, 0.2×, 0.1×, 0.05× AuNP-anti-mouse IgG solutions using Milli-Q water and 1% (v/v) blocking agent, which was applied to prevent AuNP aggregation.

Figure 4a shows a sequence of PRAM images of the 25×25 μm^2 PC active region from 0 to 60 minutes, scanned every 15 minutes. Across all AuNP-anti-mouse IgG concentrations, Figure 4b demonstrates the increased AuNP capture after 60 minutes.

AuNP attachment density was counted manually. Figure 4c quantifies the AuNP count over time for each respective AuNP-anti-mouse IgG concentration. Here, we observed nearly linear increase in particle count over time for the 0.2×, 0.1×, 0.05× AuNP samples. However, the 0.5 × AuNP sample count dramatically increases between 0 and 15 minutes, with saturation occurring by 45 minutes. In addition, all concentrations of AuNP conjugates tested can be clearly discriminated within 60 minutes. The PC reference area was utilized to estimate the nonspecific binding in the active area. Figure 4d compares the captured AuNP (0.2×) density between reference and active areas along the PC biosensor. At the 60-minute end point, the density of captured AuNPs in the reference area is ~4 × lower than that in the active area, indicating the antibody specificity of the active region. For the 0.05× AuNP conjugates, we estimate that ~13% of the total AuNP conjugates were captured by the active PC surface, which is near the COMSOL simulation capture efficiency.

We evaluated the performance of the AC+DC approach using a sandwich-based HIV-1 p24 antigen detection assay. Following the workflow described above, the p24 antigen solution was mixed and incubated for an hour with the AuNP-anti-p24 conjugates solution (0.5 × concentrated from stock solution, 4.46 pM), prior to the mixture being injected by pipette into the microfluidic cartridge inlet hole. After 30 minutes of flow (driven by the absorbing pad), the PC reference and active regions were scanned using PRAM. Figure 5a demonstrates an increasing count of nanoparticles as the p24 antigen concentration increases, measured at 30 minutes. Moreover, at each respective antigen concentration, the total reference AuNP count can be subtracted from the AuNP count in the sensing region. Following this, Figure 5b highlights the broad dynamic range of the assay, which spans over six orders of magnitude from 10 to 10^7 pg mL^{-1} (0.42 to 4.2×10^5 pM) p24 target. Our assay can achieve a LOD of 10 pg mL^{-1} that is equivalent to detecting 10^5 virions in 1 mL of plasma, representing a value consistent with the detection of HIV 3–4 weeks after infection.[47,48]

Conclusions

We report a digital resolution biomolecule detection system which integrates a self-powered PC-based microfluidic cartridge with the PRAM imaging approach. Compared with other single-molecule detection methods, such as Quanterix which uses enzymatically amplified fluorescent reporters and antibody functionalized magnetic beads,[49] or the single-molecule pull-down (SiMPull) assay using total internal reflectance fluorescence (TIRF) as the readout,[50] the AC+DC system enables simple optical digital resolution and wide dynamic range measurements of individual biomolecule events. AC+DC is not subject to the limitations of photobleaching effects, while utilizing a low-intensity LED and an inexpensive image sensor, in contrast to electron multiplying charge-coupled device (EMCCD) cameras typically required for fluorescence detection.[51] These features allow for sensitive kinetic measurements of analyte accumulation on the sensor using a compact and inexpensive detection system.

Four technical obstacles for POC diagnostics are addressed in this system: (i) Simple single step workflow: The resonant coupling of the AuNPs tags to the PC resonant wavelength enables each tag to be detected with high signal-to-noise, without the use of enzymatic amplification, thermal cycles, or wash steps, (ii) Integrated passive pumping: The flow-rate is controlled with a paper absorbing pad, thus avoiding the expense and complexity of external sources of pneumatic pressure or integrated micromechanical systems, (iii) Integrated experimental control: Separate active and reference sensor regions are used to quantify the magnitude of nonspecific binding under identical conditions, (iv) Efficient capture of low-concentration analytes on the active sensing region of a biosensor: Through utilization of the PRAM imaging-based biosensor approach, analytes may be captured over an extended surface area, rather than upon only nanometer-scale active regions of discrete sensors. Our computer models show that, even under low flow rates, activated AuNPs are captured over an extended length scale, but that PCEM images in this work can quantify the density of attached AuNPs over a 25×25 μm^2 surface area, which can be extended by tiling multiple image regions together.

Beyond a proof-of-concept demonstration of particle capture and quantification, we demonstrate sensitive (LOD = 10 pg mL^{-1}) and million-fold dynamic range HIV-1 p24 antigen detection with a 30-minute assay. We anticipate that the AC+DC assay will be compatible with detection of a wide variety of proteins, small molecules, RNA, and DNA analytes. The assay also demonstrates the potential for multiplexed detection by creating spatially separate active regions with different capture probes for specific biomarkers. Altogether, the AC+DC approach shows promise for POC detection of low concentration protein biomarkers in low-volume test samples.

Conflicts of interest

There are no conflicts to declare.

Acknowledgements

This work is supported by the National Institutes of Health (NIH) R01 AI20683, F30AI122925, and the Carl Woese Institute for Genomic Biology postdoctoral fellowship. The authors also gratefully acknowledge the Nano Sensor Groups (NSG) and staff in the Nick Holonyak, Jr. Micro and Nanotechnology Laboratory for their support.

Notes and references

1 Jung W, Han J, Choi J-W, Ahn CH. Point-of-care testing (POCT) diagnostic systems using microfluidic lab-on-a-chip technologies. Microelectronic Engineering. 2015;132:46-57.

2 Vashist SK, Luppa PB, Yeo LY, Ozcan A, Luong JHT. Emerging Technologies for Next-Generation Point-of-Care Testing. Trends Biotechnol. 2015;33(11):692-705.

3 Quesada-Gonzalez D, Merkoci A. Nanomaterial-based devices for point-of-care diagnostic applications. Chem Soc Rev. 2018;47(13):4697-709.
4 Song Y, Huang YY, Liu X, Zhang X, Ferrari M, Qin L. Point-of-care technologies for molecular diagnostics using a drop of blood. Trends Biotechnol. 2014;32(3):132-9.
5 Kelley SO, Mirkin CA, Walt DR, Ismagilov RF, Toner M, Sargent EH. Advancing the speed, sensitivity and accuracy of biomolecular detection using multi-length-scale engineering. Nat Nanotechnol. 2014;9(12):969-80.
6 Gooding JJ, Gaus K. Single-Molecule Sensors: Challenges and Opportunities for Quantitative Analysis. Angew Chem Int Ed Engl. 2016;55(38):11354-66.
7 Jin LH, Li SM, Cho YH. Enhanced detection sensitivity of pegylated CdSe/ZnS quantum dots-based prostate cancer biomarkers by surface plasmon-coupled emission. Biosens Bioelectron. 2012;33(1):284-7.
8 Huang C-S, George S, Lu M, Chaudhery V, Tan R, Zangar RC, et al. Application of Photonic Crystal Enhanced Fluorescence to Cancer Biomarker Microarrays. Analytical Chemistry. 2011;83(4):1425-30.
9 George S, Chaudhery V, Lu M, Takagi M, Amro N, Pokhriyal A, et al. Sensitive detection of protein and miRNA cancer biomarkers using silicon-based photonic crystals and a resonance coupling laser scanning platform. Lab Chip. 2013;13(20):4053-64.
10 Zhuo Y, Hu H, Chen W, Lu M, Tian L, Yu H, et al. Single nanoparticle detection using photonic crystal enhanced microscopy. Analyst. 2014;139(5):1007-15.
11 Armani AM, Kulkarni RP, Fraser SE, Flagan RC, Vahala KJ. Label-Free, Single-Molecule Detection with Optical Microcavities. Science. 2007;317(5839):783.
12 Mun KS, Alvarez SD, Choi WY, Sailor MJ. A stable, label-free optical interferometric biosensor based on TiO2 nanotube arrays. ACS Nano. 2010;4(4):2070-6.
13 Park B, Yun SH, Cho CY, Kim YC, Shin JC, Jeon HG, et al. Surface plasmon excitation in semitransparent inverted polymer photovoltaic devices and their applications as label-free optical sensors. Light: Science & Applications. 2014;3(12):e222-e.
14 Contreras Jimenez G, Eissa S, Ng A, Alhadrami H, Zourob M, Siaj M. Aptamer-based label-free impedimetric biosensor for detection of progesterone. Anal Chem. 2015;87(2):1075-82.
15 Cao X, Cao X, Guo H, Li T, Jie Y, Wang N, et al. Piezotronic Effect Enhanced Label-Free Detection of DNA Using a Schottky-Contacted ZnO Nanowire Biosensor. ACS Nano. 2016;10(8):8038-44.
16 Hofler L, Gyurcsanyi RE. Nanosensors lost in space. A random walk study of single molecule detection with single-nanopore sensors. Anal Chim Acta. 2012;722:119-26.
17 Squires TM, Messinger RJ, Manalis SR. Making it stick: convection, reaction and diffusion in surface-based biosensors. Nat Biotechnol. 2008;26(4):417-26.
18 Giljohann DA, Mirkin CA. Drivers of biodiagnostic development. Nature. 2009;462(7272):461-4.
19 Liu JN, Huang Q, Liu KK, Singamaneni S, Cunningham BT. Nanoantenna-Microcavity Hybrids with Highly Cooperative Plasmonic-Photonic Coupling. Nano Lett. 2017;17(12):7569-77.
20 Zhuo Y, Choi JS, Marin T, Yu H, Harley BA, Cunningham BT. Quantitative analysis of focal adhesion dynamics using photonic resonator outcoupler microscopy (PROM). Light: Science & Applications. 2018;7(1):9.
21 Canady TD, Li N, Smith LD, Lu Y, Kohli M, Smith AM, et al. Digital Resolution Detection of miRNA with Single Base Selectivity by Photonic Resonator Absorption Microscopy. PNAS. 2019(under revision).
22 Kokalj T, Park Y, Vencelj M, Jenko M, Lee LP. Self-powered Imbibing Microfluidic Pump by Liquid Encapsulation: SIMPLE. Lab Chip. 2014;14(22):4329-33.
23 Dal Dosso F, Decrop D, Pérez-Ruiz E, Daems D, Agten H, Al-Ghezi O, et al. Creasensor: SIMPLE technology for creatinine detection in plasma. Analytica Chimica Acta. 2018;1000:191-8.
24 Wang J, Ahmad H, Ma C, Shi Q, Vermesh O, Vermesh U, et al. A self-powered, one-step chip for rapid, quantitative and multiplexed detection of proteins from pinpricks of whole blood. Lab on a Chip. 2010;10(22).
25 Cunningham BT, Li P, Schulz S, Lin B, Baird C, Gerstenmaier J, et al. Label-free assays on the BIND system. J Biomol Screen. 2004;9(6):481-90.
26 Cunningham B, Lin B, Qiu J, Li P, Pepper J, Hugh B. A plastic colorimetric resonant optical biosensor for multiparallel detection of label-free biochemical interactions. Sensors and Actuators B: Chemical. 2002;85(3):219-26.
27 Shafiee H, Lidstone EA, Jahangir M, Inci F, Hanhauser E, Henrich TJ, et al. Nanostructured optical photonic crystal biosensor for HIV viral load measurement. Sci Rep. 2014;4:4116.
28 Race CM, Kwon LE, Foreman MT, Huang Q, Inan H, Kesiraju S, et al. An Automated Microfluidic Assay for Photonic Crystal Enhanced Detection and Analysis of an Antiviral Antibody Cancer Biomarker in Serum. IEEE Sensors Journal. 2018;18(4):1464-73.
29 Huang Q, Cunningham BT. Microcavity-Mediated Spectrally Tunable Amplification of Absorption in Plasmonic Nanoantennas. Nano Letters. 2019.
30 Hosokawa K, Sato K, Ichikawa N, Maeda M. Power-free poly(dimethylsiloxane) microfluidic devices for gold nanoparticle-based DNA analysis. Lab Chip. 2004;4(3):181-5.
31 Dimov IK, Basabe-Desmonts L, Garcia-Cordero JL, Ross BM, Park Y, Ricco AJ, et al. Stand-alone self-powered integrated microfluidic blood analysis system (SIMBAS). Lab Chip. 2011;11(5):845-50.
32 Liang DY, Tentori AM, Dimov IK, Lee LP. Systematic characterization of degas-driven flow for poly(dimethylsiloxane) microfluidic devices. Biomicrofluidics. 2011;5(2):24108.
33 Juncker D, Schmid H, Drechsler U, Wolf H, Wolf M, Michel B, et al. Autonomous microfluidic capillary system. Anal Chem. 2002;74(24):6139-44.
34 Zimmermann M, Schmid H, Hunziker P, Delamarche E. Capillary pumps for autonomous capillary systems. Lab Chip. 2007;7(1):119-25.
35 Safavieh R, Tamayol A, Juncker D. Serpentine and leading-edge capillary pumps for microfluidic capillary systems. Microfluidics and Nanofluidics. 2014;18(3):357-66.
36 Safavieh R, Juncker D. Capillarics: pre-programmed, self-powered microfluidic circuits built from capillary elements. Lab Chip. 2013;13(21):4180-9.
37 Gubala V, Harris LF, Ricco AJ, Tan MX, Williams DE. Point of Care Diagnostics: Status and Future. Analytical Chemistry. 2011;84(2):487-515.
38 Nisar A, Afzulpurkar N, Mahaisavariya B, Tuantranont A. MEMS-based micropumps in drug delivery and biomedical applications. Sensors and Actuators B: Chemical. 2008;130(2):917-42.
39 Romoli L, Tantussi G, Dini G. Experimental approach to the laser machining of PMMA substrates for the fabrication of microfluidic devices. Optics and Lasers in Engineering. 2011;49(3):419-27.
40 Xiong R, Chung JN. Flow characteristics of water in straight and serpentine micro-channels with miter bends. Experimental Thermal and Fluid Science. 2007;31(7):805-12.

41 Green JV, Kniazeva T, Abedi M, Sokhey DS, Taslim ME, Murthy SK. Effect of channel geometry on cell adhesion in microfluidic devices. Lab Chip. 2009;9(5):677-85.
42 Karale CM, Bhagwat SS, Ranade VV. Flow and heat transfer in serpentine channels. AIChE Journal. 2013;59(5):1814-27.
43 Tan Y, Tang T, Xu H, Zhu C, Cunningham BT. High sensitivity automated multiplexed immunoassays using photonic crystal enhanced fluorescence microfluidic system. Biosens Bioelectron. 2015;73:32-40.
44 Kirby BJ. Micro-and nanoscale fluid mechanics: transport in microfluidic devices. : Cambridge university press; 2010.
45 Whitaker S. Flow in porous media i: a theoretical derivation of darcy's law. Transport in Porous Media. 1986;1(1):3-25.
46 Fu E, Ramsey SA, Kauffman P, Lutz B, Yager P. Transport in two-dimensional paper networks. Microfluid Nanofluidics. 2011;10(1):29-35.
47 Fiebig EW, Wright DJ, Rawal BD, Garrett PE, Schumacher RT, Peddada L, et al. Dynamics of HIV viremia and antibody seroconversion in plasma donors: implications for diagnosis and staging of primary HIV infection. AIDS. 2003;17(13):1871-9.
48 Cohen MS, Gay CL, Busch MP, Hecht FM. The detection of acute HIV infection. J Infect Dis. 2010;202 Suppl 2:S270-7.
49 Rissin DM, Kan CW, Campbell TG, Howes SC, Fournier DR, Song L, et al. Single-molecule enzyme-linked immunosorbent assay detects serum proteins at subfemtomolar concentrations. Nat Biotechnol. 2010;28(6):595-9.
50 Jain A, Liu R, Ramani B, Arauz E, Ishitsuka Y, Ragunathan K, et al. Probing cellular protein complexes using single-molecule pull-down. Nature. 2011;473(7348):484-8.
51 Cunningham BT, Zhang M, Zhuo Y, Kwon L, Race C. Recent Advances in Biosensing With Photonic Crystal Surfaces: A Review. IEEE Sens J. 2016;16(10):3349-66.

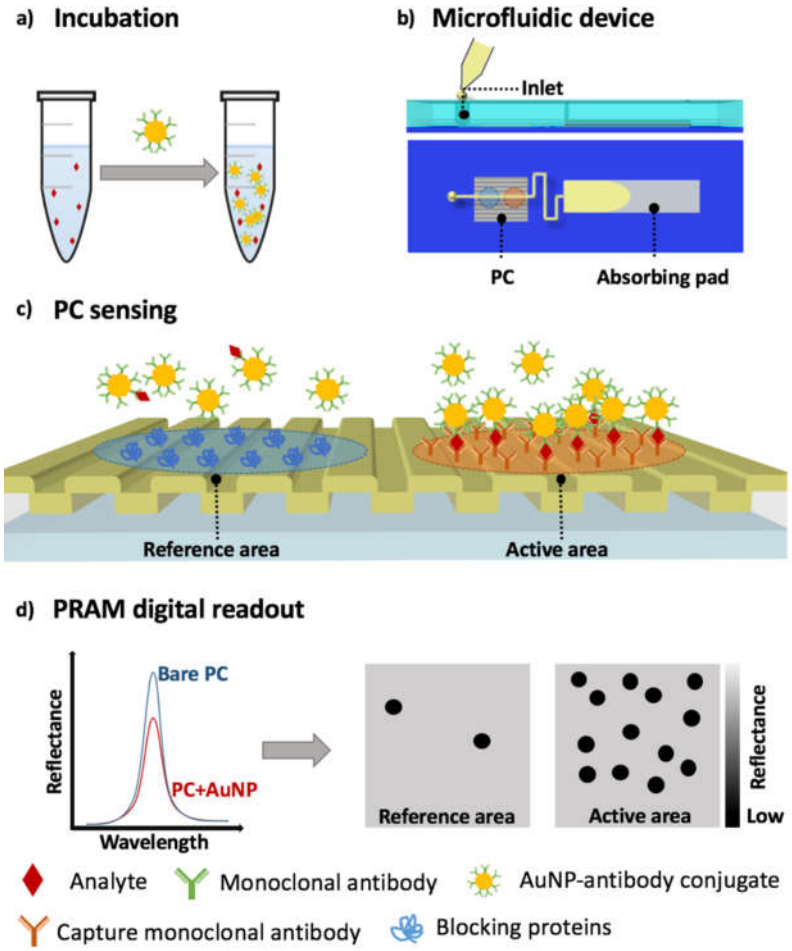

Figure 1 Workflow of the AC+DC assay in a microfluidic cartridge. (a) The test sample is mixed and incubated with an excess of AuNP-antibody conjugates. (b) The mixture is introduced into a microfluidic device which is comprised of a PC for sensing and an absorbing pad for pumping. (c) The PC reference area (blue) is blocked with proteins to prevent non-specific binding and the PC active area is functionalized with capture monoclonal antibodies. The analyte is sandwiched between the AuNP conjugate and the immobilized capture antibody on the PC surface. (d) The sensing regions are scanned using PRAM. High contrast and digital resolution images are obtained by the detection of the reflected intensity drop caused by the local nanoparticle binding.

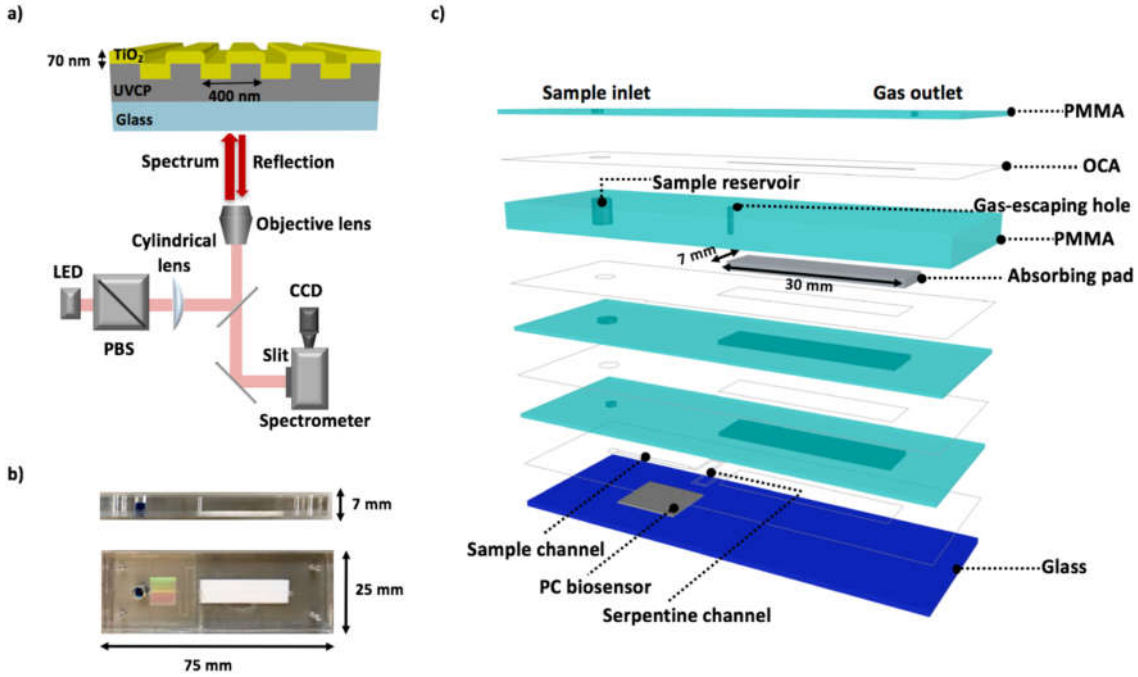

Figure 2 (a) Schematic of the microfluidic photonic resonator absorption microscopy (PRAM) instrument. (b) Photo of the fully assembled microfluidic cartridge. (c) An expanded schematic of the microfluidic cartridge, which is comprised of patterned PMMA and adhesive layers (OCA). PMMA sheets are utilized to create a reservoir for the test sample and a cavity for the absorbing pad. Adhesive layers are used to sandwich PMMA sheets and provide channels for fluid. After all layers and the absorbing pad are aligned and pressed together, a functionalized PC biosensor is attached to the bottom with adhesive.

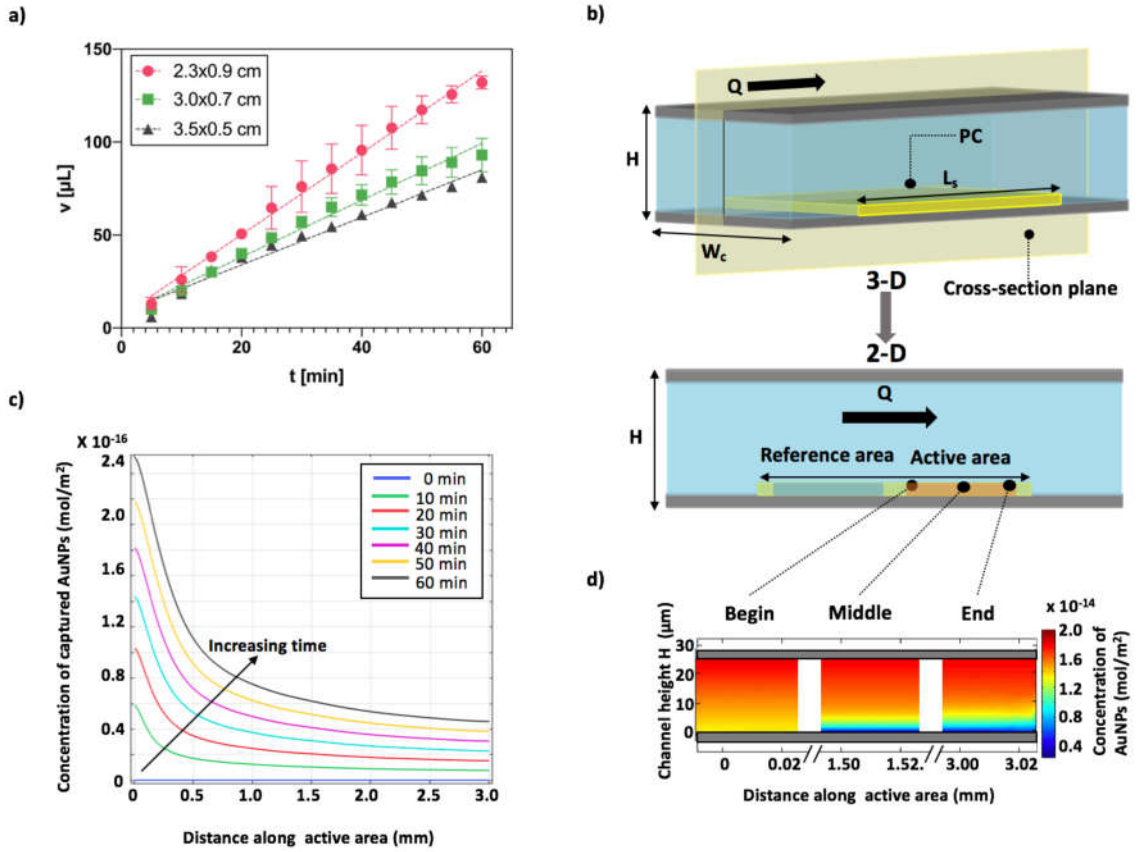

Figure 3 The optimization and modulation of the microfluidic device. (a) Characterization of the flow rate modulation by adjusting the dimensions of the absorbing pad. The filter paper pad was cut into rectangles with various lengths and widths: 2.3 × 0.9 cm (red, ∂=0.39), 3 × 0.7 cm (green, ∂=0.23) and 3.5 × 0.5 cm (black, ∂=0.14). Results indicate the volume flow rate is constant, and increasing with the increase of ∂. (b) The COMSOL modeled domain is the 2-D cross-section plane of the 3-D sample channel with a PC biosensor at the bottom, where Q represents the liquid flow direction. (c) The concentration of captured AuNPs increases over time, and the highest density of AuNP capture is predicted to occur at the leading edge of the active area. (d) The concentration of target molecules at the beginning, middle, and end of the active area with a channel height of 25 mm at 60 minutes. Our model predicts an overall ~20% average capture efficiency for activated AuNPs within the active area of the sensor.

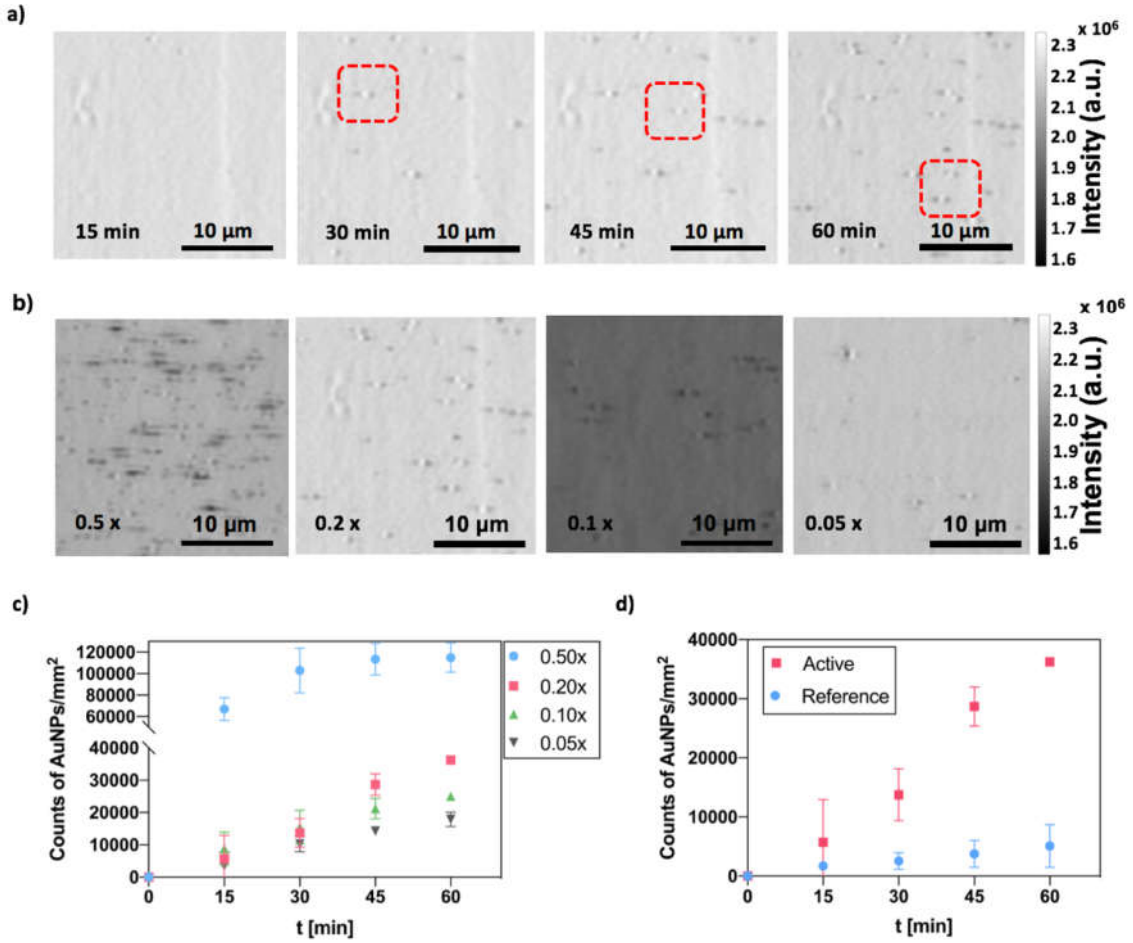

Figure 4 Imaging and quantification of AuNPs by the microfluidic photonic resonator absorption microscopy (PRAM) system. (a) A series of peak intensity value PRAM images of the PC active area indicate the increased count of AuNPs (Example AuNP indicated in the red dashed box. An explanation of the observed patterns for captured AuNPs by PRAM is provided in Supplementary Notes) over 60 minutes with 0.2× concentrated AuNP conjugates. (b) The PRAM images of the PC active area with addition of different concentrations of AuNP conjugates samples. (c) The quantification of the captured AuNPs density over time for each AuNP conjugate concentration. (d) The comparison of the captured AuNP density change between reference and active areas over time. Each data point represents the average of 3 independent experiments. Error bars represent the standard errors.

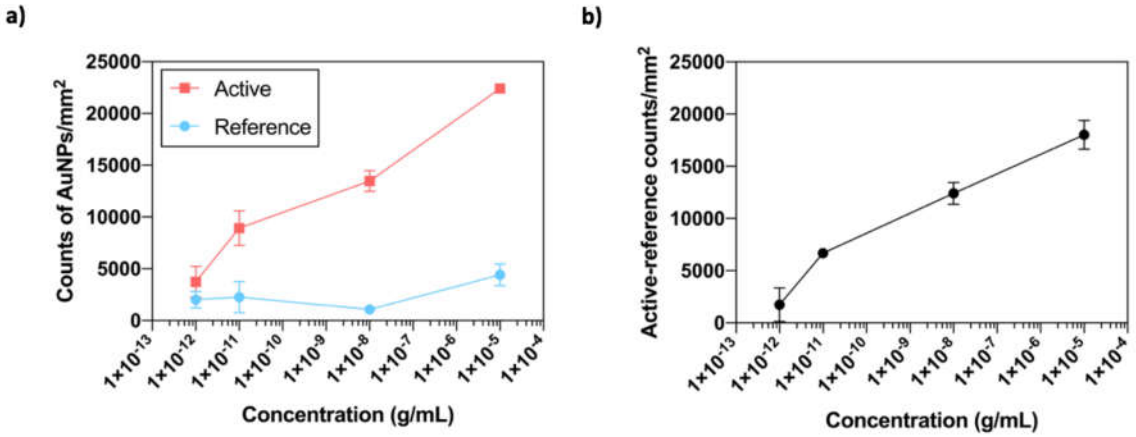

Figure 5 HIV-1 p24 detection. (a) The comparison of the captured AuNP density in the reference and active areas with increasing p24 antigen concentration at 30 minutes. (b) By subtracting the reference count from the active count, we observe a broad linear dynamic range for the p24 assay. Each data point represents the average of 3 independent experiments. Error bars represent the standard errors.

Supplementary Information

Activate Capture and Digital Counting (AC+DC) assay for protein biomarker detection integrated with a self-powered microfluidic cartridge

Congnyu Che[a], Nantao Li[b], Kenneth D. Long[a], Miguel Angel Aguirre[c], Taylor D. Canady[d], Qinglan Huang[b], Brian T. Cunningham[a,b,d,*]

a. Department of Bioengineering, University of Illinois at Urbana-Champaign, 208 North Wright Street, Urbana, IL 61801, USA

b. Department of Electrical and Computer Engineering, University of Illinois at Urbana-Champaign, 208 North Wright Street, Urbana, IL 61801, USA

c. Department of Analytical Chemistry and Food Science and University Institute of Materials, Faculty of Science, University of Alicante, 03080 Alicante, Spain

d. Carl R. Woese Institute for Genomic Biology, University of Illinois at Urbana-Champaign, 1206 West Gregory Drive, Urbana, IL 61801, USA

1. Resonant reflection spectrum of the PC biosensor

The resonant reflection spectrum from one pixel of a PRAM image is shown in Supplementary Figure 1 with and without an attached gold nanoparticle (AuNP), indicating a reflected intensity reduction of 22% when the AuNP is observed.

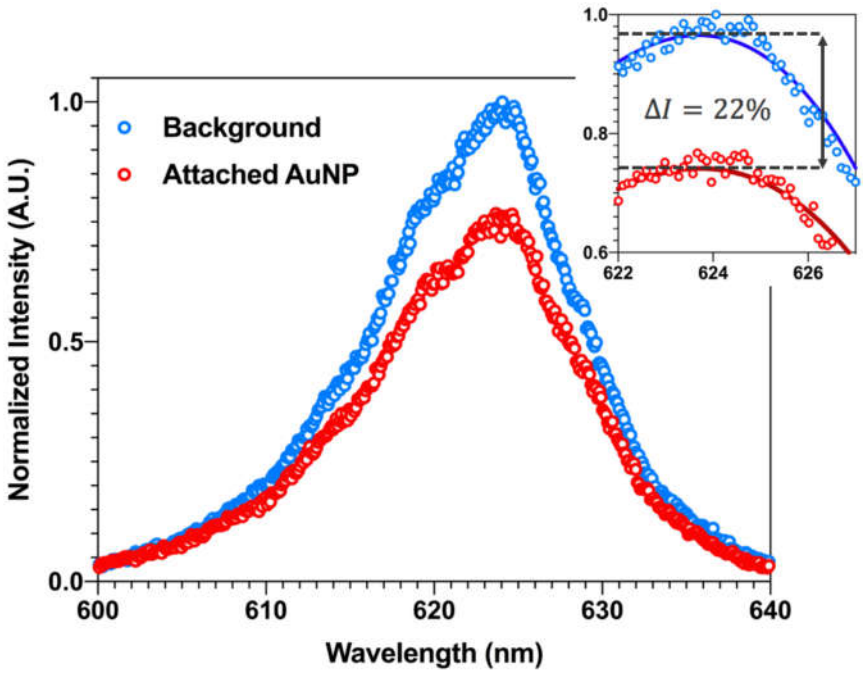

Supplementary Figure 1. Example spectrum with a reflected intensity change with/without an attached AuNP. Inset: Zoomed in image of the normalized spectrum with third order polynomial fitting (background fitting in blue line, AuNP fitting in red line).

2. AuNP patterns on the PRAM image

The elongated patterns observed on the PRAM images originate from the non-uniform enhanced field on the photonic crystal (PC) surface. Specifically, the PC grating periodicity is oriented in the vertical direction in our images, and thus the PC resonant electromagnetic field intensity is periodic in the horizontal direction, while uniform in the vertical direction. The periodic illumination patterns shifts the center of the Fourier plane towards higher frequencies,[1] resulting in the observed side lobes in the image, surrounding each surface-bound AuNP on its left and right sides. In addition, the vertical distance between the nanoparticle and the PC surface can induce either a reduced intensity or an increased intensity at the central location of the AuNP. While this

topic is outside the scope of the present manuscript, a brief description of this phenomenon is as follows: AuNPs attached to the PC with a vertical separation distance of several nanometers induce efficient quenching the PC resonant electromagnetic field, and thus we observe a prominent dark spot in the reflected intensity from the location at which the AuNP is present. However, depending upon the precise orientation of the capture antibody on the AuNP and the secondary antibody on the PC, it is possible that the proteins will displace the AuNP in the vertical direction by ~30-50 nm. Numerical simulations of vertically displaced AuNPs reveals that this situation leads to constructive interference between light scattered by the AuNP and the reflected light from the PC structure, resulting in the greater intensity at the center of the AuNP, as demonstrated in Supplementary Figure 2.[2] This phenomenon opens the potential for utilizing the PRAM intensity to measure vertical displacements of single biomolecular interactions, which is an interesting topic outside the scope of this work. Here, we count both dark-centered and bright-centered AuNP patterns to generate our quantitative assay output.

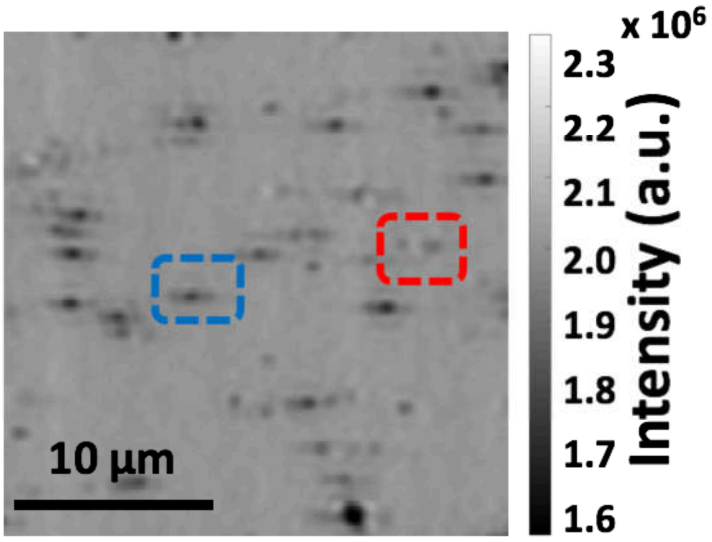

Supplementary Figure 2. PRAM image of AuNPs. The AuNP patterns are composed of two side lobes with either bright center (red dashed box), or a dark center (blue dashed box).

3. AuNP-IgG conjugation solution

The IgG conjugated AuNP (AuNP-IgG) solution was prepared by adding 12 µL of SH-PEG-IgG solution to 200 µL of stock AuNP solution. The SH-PEG-IgG solution was added in a series of small volumes (4µL), and the hydrodynamic diameter of AuNU-IgG conjugates was were measured by Dynamic Light Scattering (model DelsaMax Pro, Beckman Coulter, Pasadena, CA, USA). Figure 3 shows the hydrodynamic diameter of AuNPs in solution before and after adding incremental volumes of SH-PEG-IgG. 12 µL of SH-PEG-IgG was selected to ensure optimal bioconjugation, representing the point at which AuNPs reached their binding capacity.

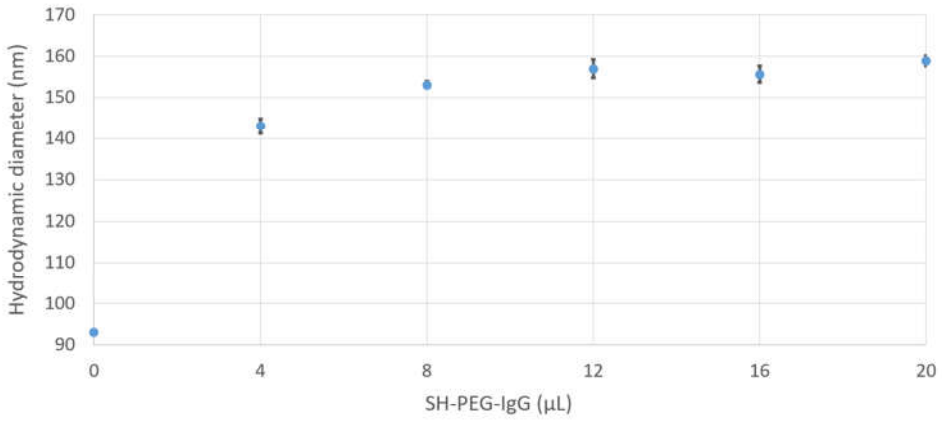

Supplementary Figure 3. Relationship between hydrodynamic diameter of AuNPs in solution and the volume of SH-PEG-IgG, used to determine conditions that result in full occupancy of binding for IgG on the AuNP surface.

4. COMSOL simulation parameters and governing equations

We demonstrate a 2-D cross-section model to simulate the transport and adsorption of biomolecules on the PC biosensor embedded in the microfluidic cartridge. The Transport of Diluted Species (tds) and the General Form Boundary PDE (gb) physics are coupled together to

solve this mass balance problem. The parameters involved in this simulation are shown in Table 1. The mass balance for the PC biosensor surface, including surface diffusion and the reaction rate expression for the generation of the absorbed AuNPs, C_s, is:

$$\frac{\partial C_s}{\partial t} + \nabla \cdot (-D_s \nabla C_s) = k_{on} c(\Gamma_s - c_s) - k_{off} c_s \quad (1)$$

Where D_s is the surface diffusivity, and Γ_s is the total surface concentration of the active sites. With the coupling between two mass transfer mechanisms (diffusion and surface adsorption), we define the boundary conditions of the AuNPs transport in the microfluidic channel as:

$$c = c_0 \quad \text{at the inlet} \quad (2)$$

$$\vec{n} \cdot (-D\nabla \mathrm{c} + \mathrm{c}\vec{u}) = 0 \quad \text{at the microfluidics channel walls and inactivated sites} \quad (3)$$

$$\vec{n} \cdot (-D\nabla \mathrm{c} + \mathrm{c}\vec{u}) = -k_{on} c(\Gamma_s - c_s) + k_{off} c_s \quad \text{at the PC biosensor active area} \quad (4)$$

$$\vec{n} \cdot (-D\nabla \mathrm{c} + \mathrm{c}\vec{u}) = \vec{n} \cdot \mathrm{c}\vec{u} \quad \text{at the outlet} \quad (5)$$

Where $\vec{n}$ is the unit normal vector directed out of a surface, and $\vec{u}$ is the velocity of the fluid. Boundary condition (2) constrains the AuNP solution injected into the channel to have constant concentration c_0. Boundary (3) ensures that no AuNP can diffuse out of the channel walls. Boundary condition (4) describes the binding kinetics at the PC active area, considering the rate of the reaction at the active area, the flux of the AuNPs, and the concentration of absorbed AuNPs.

Table 1. Parameters for COMSOL 2-D model

Name	Value	Description
C_o	1.66×10^{-17} mol L^{-1}	Initial concentration of AuNPs
k_{on}	1×10^{6} M^{-1} s^{-1}	Typical value for k_{on}
k_{off}	1×10^{-5} s^{-1}	Typical value for k_{off}
b_{max}	2×10^{-8} kg m^{-2}	Active site concentration

D_s	1×10^{-11} m^2 s^{-1}	Surface diffusivity
D	3.8×10^{-12} m^2 s^{-1}	AuNPs diffusivity
H	2.5×10^{-5} m	Channel height
W_c	5×10^{-4} m	Channel width
L	9×10^{-3} m	Channel length
V_{max}	0.0018 m s^{-1}	Maximum velocity

References

1. Wei F, Liu Z. Plasmonic structured illumination microscopy. Nano Lett. 2010;10(7):2531-6.

2. Sevenler D, Daaboul GG, Ekiz Kanik F, Unlu NL, Unlu MS. Digital Microarrays: Single-Molecule Readout with Interferometric Detection of Plasmonic Nanorod Labels. ACS Nano. 2018;12(6):5880-7.